Dual strategy for reduced signal-suppression effects in matrix-assisted laser desorption/ionization mass spectrometry imaging

Bastrup, Joakim; Birkelund, Svend; Asuni, Ayodeji; Volbracht, Christiane; Stensballe, Allan

Published in:
Rapid communications in mass spectrometry : RCM

DOI (link to publication from Publisher):
10.1002/rcm.8521

Publication date:
2019

Document Version
Accepted author manuscript, peer reviewed version

Bastrup Joakim (Orcid ID: 0000-0002-4292-5234)
Stensballe Allan (Orcid ID: 0000-0002-9888-1955)

Dual strategy for reduced signal suppression effects in MALDI mass spectrometry imaging.

Running title:
Dual strategy for reduced signal suppression effects in MALDI imaging

Bastrup, Joakim

- Aalborg Universitet Institut for Medicin og Sundhedsteknologi

- H Lundbeck A/S, Neuroscience

Birkelund, Svend

-Aalborg University, Department of Health Science and Technology

Asuni, Ayodeji

-H Lundbeck A/S, Neuroscience

Volbracht, Christiane

-H Lundbeck A/S, Neuroscience

Stensballe, Allan

-Aalborg Universitet Institut for Medicin og Sundhedsteknologi

Corresponding author:
Allan Stensballe: Aalborg University. Department of Health Science and Technology. Fredrik Bajers Vej 7. Building: E, Room: E4-114. 9220 Aalborg East. Denmark. Phone: +45 61 60 87 86.

This article has been accepted for publication and undergone full peer review but has not been through the copyediting, typesetting, pagination and proofreading process which may lead to differences between this version and the Version of Record. Please cite this article as doi: 10.1002/rcm.8521

Contact information:
Joakim Bastrup: jbas@hst.aau.dk ; joak@lundbeck.com

Svend Birkelund: sbirkelund@hst.aau.dk

Ayodeji A. Asuni: aara@lundbeck.com

Christiane Volbracht: cvo@lundbeck.com

Allan Stensballe: as@hst.aau.dk

Introduction

Matrix-assisted laser desorption-ionization mass spectrometry imaging (MALDI imaging) has advanced and is capable of visualizing diverse molecular alteration signatures in tissue sections[1,2]. The MALDI imaging technology is, in contrast to traditional immunohistochemistry, an antibody-independent technology which can be utilized to localize small molecules, lipids, peptides and proteins following a single analysis. MALDI imaging requires highly optimized conditions for optimal data acquisition for each class of biomolecule. One key issue is signal suppression effects which reduces the ionization of analytes, particularly in complex mixtures. This effect has been reported previously when analyzing simple specimens on a MALDI target plate[3] and occurs to a higher degree when analyzing a complex tissue section. Signal suppression effects can arise from several sources e.g. by a variable degree of analyte ionization efficiency or presence of ion suppressing molecules such as salts, alkali-metals and lipids that competes with the ionization[4]. Further, post-translational modified peptides are known to empirically ionize significantly less efficient than un-modified counterparts[5,6]. Strategies to counteract these issues are critical for obtaining optimal results in MALDI imaging especially for biological specimens. Optimizations include sample pretreatment steps, such as sample handling, washing, matrix chemical and deposition and parallel approaches like laser capture microdissection to accumulate of discrete target material directly from tissue sections. Different solubilized MALDI matrices, such as sinapinic acid (SA;[7]), α-cyano-4-hydroxycinnamic acid (CHCA;[8]) and 2,5-dihydroxybenzoic acid (DHB;[9]), gave rise to high quality mass spectra of peptide and protein containing specimens. Different matrix additives and organic acids e.g. trifluoroacetic acid (TFA) improved the matrix capabilities and robustness[10–12]. All implying that enhanced sensitivity and improved reproducibility is achievable by homogenous crystal size, analyte embedding and reducing the effects of alkali-metal and salts. The development of the 'super-DHB' matrix (S-DHB) improved matrix properties by increasing the S/N ratios of membrane protein samples

containing contaminants[13] in MALDI-MS further. The matrix is a mixture of 2,5-DHB and 2-hydroxy-5-methoxybenzoic acid (9:1; w/w;[11,13,14]). The combinatory effect of adding phosphoric acid (PA) to the DHB matrix significantly enhanced the detection of phosphopeptides and non-phosphopeptides by reducing adduct formation (e.g. alkali-metal adducts) and thus signal suppression[5,6,12,15]. These techniques were applied in previous MALDI-MS studies but not in MALDI imaging. We reason that such capabilities are advantageous especially in MALDI imaging on complex tissue material with high background inducing signal suppression (e.g. brain tissue sections having high lipid content).

Alzheimer's disease (AD) is a progressive neurodegenerative disorder that affects memory and cognition and is the most common cause of dementia in the elderly. Extracellular amyloid plaques composed mainly of 38–43 residue beta-amyloid (Aβ) peptides are a histopathological hallmark of AD[16]. Aβ peptides originate from sequential cleavage of the membrane-spanning amyloid precursor protein (APP). Based on the 'amyloid cascade hypothesis' a chronic imbalance between production and clearance of Aβ peptides leads to increased levels and an excessive deposition of Aβ peptides into amyloid plaques[17,18], eventually resulting in neuronal dysfunction and dementia [19–21]. Transgenic (tg) mouse models have been developed to mimic amyloid pathology observed in AD. These models are based on familial AD (FAD) mutations which cause an increased Aβ load and early-onset inherited AD in humans[22].

Aβ peptides associated with amyloid plaques in brain tissue from both tg mouse models and AD have been investigated by MALDI imaging previously. However, Aβ species coverage and signal-to-noise (S/N) ratios have been highly diverging and variable peptide compositions have been reported[23–30], making it difficult to conclude on the different study results. We reason that eliminating the issue of signal suppression in brain tissue could improve robustness and comparability of MALDI imaging analysis of amyloid plaques.

In this study, we investigated Aβ plaques with MALDI imaging by combining two parallel approaches that together provide a novel strategy for overcoming signal suppression: 1) Laser microdissection to extract and accumulate Aβ plaques and 2) PA as additive to the S-DHB matrix. Both strategies were integrated to investigate whether signal suppression effects hampering MALDI imaging analysis of Aβ proteoforms previously could be counteracted. We analyzed Aβ proteoforms from postmortem AD brains and tg APPPS1-21 mice overexpressing FAD mutations in APP and presenilin-1 (PS1)[31]. Laser microdissection allowed extraction and accumulation of thioflavin-T stained Aβ plaques. The enrichment improved matrix:analyte ratio, enabled tandem MS fragmentation analysis and comparison of PA and TFA as matrix

additives to the S-DHB matrix. PA added to the S-DHB matrix, improved the S/N ratio of several m/z values, including Aβ1-42 (m/z range: 4300-4900), compared to CHCA, SA and S-DHB containing TFA as matrix additive in our MALDI imaging analysis. PA addition improved the analysis of Aβ proteoforms specially from AD brain enabling us to investigate several significant differences in Aβ plaque composition isolated from AD compared to APPPS1-21 brains.

Experimental.

Chemicals

Chloroform (99%), methanol (MeOH; 99%), acetonitrile (ACN; 99%), acetic acid (100%), phosphoric acid (PA; 85 wt. % in H_2O), S-DHB (99%) and CHCA (99%) matrices were purchased from (Sigma Aldrich; Denmark). The SA matrix was purchased from (Bruker Daltonics; Germany), formic acid (FA; 98%) was purchased from (Fluka; Denmark), TFA (99%) was purchased from (Fisher Scientific; Denmark) and thioflavin-T from (Merck Eurolab; Denmark).

Human brain tissue

Prefrontal cortex (PFC) regions from five AD patients (two males and three females) were obtained from Tissue Solutions Ltd (Scotland). The tissue specimens were collected at a postmortem interval between 2-20 hours, snap frozen and stored at -80°C. The specimens were pathologically staged according to Braak and Braak[32] and staged between V and VI. Four of the patients had reported history of AD in their families.

Animal brain tissue

Three 9-month old female APP transgenic mice (APPPS1-21) were used for the analysis (Charles River; Germany)[31]. The mice were group-housed (five/cage). Water and food were supplied *ad libitum*, clean cages were provided twice a week and mice were kept on a 12hr/12hr light/dark schedule. Room humidity was 55%±5%, and room temperature (RT) was 21±2°C. All animal experiments were performed in accordance with Danish legislation and animal welfare laws.

The mice were euthanized by decapitation. The brains were extracted, split into two hemispheres with a razor blade, frozen with dry ice and stored at -80°C. Brain tissue used for MALDI imaging analysis were cut into 12-µm thick sagittal sections using a cryostat microtome (Leica CM3050 S) and attached to Indium tin oxide (ITO) coated glass slides (Bruker Daltonics; Germany). Brain tissue used for laser capture microdissection was cut into

25-µm thick sagittal sections and attached to a polyethylene naphthalate (PEN) membrane glass slide (Thermo Fisher; Denmark). The glass slides (both ITO coated and PEN membrane) containing tissue sections were fixated in 70% EtOH and 99% EtOH for one minute in each solution and allowed to dry at RT. The slides were then stored at -80°C until further use.

Sample preparation for MALDI imaging

The glass slides containing the attached sections were dried at RT in a vacuum desiccator for 30 minutes. Next, they were rinsed in a series of solutions: 70% EtOH, 99.9% EtOH, Carnoy's fluid (EtOH, chloroform, acetic acid (60/30/10, v:v:v), 99.9% EtOH, ddH2O, 99.9% EtOH. The glass slides were left for 30 seconds in EtOH and ddH2O and two minutes in Carnoy's fluid[33]. They were subsequently left to dry for 45 minutes in a vacuum desiccator.

Matrix deposition

Three matrices (CHCA, SA and S-DHB) were chosen for the comparison. The CHCA matrix (7 mg/ml) was dissolved in 50:50:0.2 (v:v:v) ACN:ddH_2O:TFA. The S-DHB matrix (30 mg/ml) was dissolved in 50:50:0.2 (v:v:v) MeOH:ddH_2O:TFA or PA. The SA matrix (10 mg/ml) was dissolved in 60:40:0.2 (v:v:v) ACN:ddH_2O:TFA.

The matrices were deposited by using the ImagePrep robot (Bruker Daltonics) and company provided default deposition programs (DHB_nsh04 for S-DHB, HCCA_nsh04 for CHCA and SA_nsh04 for SA). Data logger software was used together with a coverslip (Bruker Daltonics) added on top of the glass slides to further validate and improve the deposition (Supplementary Figure 1). Average values acquired from the matrix deposition were manually noted and listed in (Table 1).

Laser capture microdissection of plaque regions

The PEN membrane glass slide containing one brain tissue section from each APPPS1-21 mouse was dried at RT for 25 minutes, dip washed in ddH_2O and stained in 1% thioflavin-T solution for 10 minutes in darkness. The sections were washed in ddH_2O for three minutes three times and dried at RT for 1 hour. The Veritas laser microdissection instrument (Arcturus Bioscience) was utilized to microdissect plaques and adjacent control regions from each brain section. The microdissected material was collected in CapSure^{TM} Macro LCM caps (Thermo Fisher). On average, 36 plaques corresponding to an area of 123.9 µm^2 and 35 adjacent control regions corresponding to an area of 251.4 µm^2 were extracted per section. The sample material was extracted from the caps by adding and resuspending 15 µl of 70% FA/ddH_2O on the cap surface three times followed by incubation in the 70% FA solution O/N at 37°C. Next, the

tubes were inserted into a SpeedVac (miVac, GeneVac) for 3 hours and stored at -80°C until further use. The dried material was reconstituted in 12 µl 20% ACN/ 0.1% FA solution. The samples were prepared on a MALDI target plate (Bruker Daltonics) with the dried droplet method by applying 1 µl of sample material and subsequently mixing with 1 µl of S-DHB/PA or S-DHB/TFA matrix solutions.

Data acquisition

MALDI imaging data was acquired in linear positive mode optimized for imaging average masses in the m/z 1-20 kDa range (UltrafleXtreme MALDI TOF/TOF, Bruker Daltonics, Germany). A Smartbeam-II laser system (Nd:YAG 355 nm) was used. Further, the laser repetition rate was set to 1 kHz and 500 shots per spot. The detector gain voltage was set to 2887 V and 2514 V for linear and reflectron mode, respectively. The pulsed ion extraction (PIE) was set to 250 ns. Furthermore, the laser diameter was set to medium and the raster step size to 300 µm in the matrix comparison experiment. Realtime smoothing was set to medium, baseline offset adjustment was set to 0.0% and sample rate and digitizer setting was set to 1.25 GS/s. The same settings were used for the analysis of the human tissue material except the raster step size which was set to 200 µm.

MALDI-MS data was acquired in reflector positive mode optimized for the isotopic resolution in the m/z range 800-6000 Da. A total of 5000 shots per sample spot were used with a medium laser diameter and complete sample function to cover the entire spot. The laser repetition rate was set to 1 kHz and PIE was set to 170 ns.

A ClinProt Standard was used to generate calibration spectra for all conditions. This was composed of a mixture (1:1) of Protein Calibration Standard I and Peptide Calibration Standard II (Bruker Daltonics, Germany) and consisted of the following references: ACTH_clip (1-17) 2094.42700 Da; ACTH_clip (18-39) 2466.68100 Da; Somatostatin (28) 3149.57300 Da; Insulin 5734.51800 Da; Ubiquitin I 8565.76400 Da; Cytochrom C 12360.97400 Da; Myoglobin 16952.30600 Da.

Aβ1–42 was synthesized according to Axelsen et al. (2009) with standard procedures using Fmoc-strategy on an automatic ABI 433 synthesizer (Applied Biosystems)[34]. The mass of the synthesized peptide was analyzed by MALDI-TOF (Autoflex, Bruker Daltonics, Germany). The peptide was subsequently purified by preparative high performance liquid chromatography, on a SymmetryPrep TM C18 7 µm, 7.8 × 300 mm column (Waters; United Kingdom) by collecting the main peak, which was then subjected to analytical HPLC using a

Symmetry C18 5 µm, 4.6 × 25 cm column (Waters; United Kingdom) and the fractions were subsequently lyophilized.

The Aβ1-42 peptide was added adjacent to the calibration standard and used to verify the m/z value and tandem MS fragmentation pattern of Aβ1-42 in the tissue sections prior to the analysis.

Data processing of mass spectrometry spectra

Matrix comparison

The data files were imported into SCiLS Lab software (v2017a, Bruker Daltonics, Germany) where data for the statistical analysis was extracted. In brief, the *.mis* files obtained in FlexImaging (v4.0) were imported to SCiLS Lab and processed by top hat baseline correction (width: 200) and TIC normalization. Brain sections (both tg mouse and human) were grouped into their respective matrix treatment (S-DHB/PA, S-DHB/TFA, SA/TFA and CHCA/TFA) and the *Find Peaks* function was used on the different groups to identify peaks. The report table was used to export the average peak information per matrix condition (centroid (m/z); add mean intensities; maximum intensity in interval; standard deviation at maximum, m/z at maximum and area under curve).

Regions of interest (ROIs) with increased presence of selected Aβ species were isolated and used for statistical analysis. The normal distributed data was analyzed with two-tailed paired t-test ($p < 0.05$). A similar approach was used to create the enriched Aβ1-42 mass spectra. In brief, peaks corresponding to the calculated mass of the Aβ1-42 peptide were highlighted to visualize the spatial localization. The three highest intensity spots where selected for each brain tissue section and used to create a combined mass spectrum containing a total of 27 spots (mouse) and 30 spots (human) with the S-DHB/PA matrix. The intensity bar was adjusted in case of no clear visualization of the corresponding m/z value.

Laser microdissection and LIFT analysis

GPMAW software (v. 8.20; Lighthouse data) was used to compare the acquired mass spectra from the LIFT analysis to an in-silico fragment tandem MS of the Aβ1-42 peptide.

Data acquired from the laser microdissected plaque extract analysis was imported to Flex Analysis and individually processed with smooth function, baseline subtraction and find mass list functions. The signal-to-noise (S/N) value of the peaks corresponding to the Aβ1-42 peptide (Aβ1-42; $[M+H]^+_{mono} = 4512.2774$) was noted and adjacent peaks were matched to known Aβ

peptide variants including possible modifications using the modification list at www.unimod.org and GPMAW software.

The MALDI imaging data of the mouse brain tissue have been deposited to the ProteomeXchange Consortium via the PRIDE[35] partner repository with the dataset identifier PXD009353.

Results and Discussion

Improved detection of Aβ1-42 by laser microdissection and the matrix additive PA

Aβ plaques visualized with thioflavin-T staining were observed in the cerebral cortex of 9-month old APPPS1-21 mice (Figure 1A) confirming previous reports[31]. Thioflavin-T stained plaques were laser microdissected from indicated areas as shown in (Figure 1A). This enrichment by laser microdissection was necessary as Aβ peptides were difficult to identify with MALDI imaging in previous pilot studies due to restricted plaque areas and also likely to other molecules than Aβ peptides from the tissue which could suppress the Aβ signal (data not shown).

The analysis of the microdissected material was acquired on a MALDI target plate in reflector mode enabling acquisition of monoisotopic masses with high intensities. From the Aβ plaque analysis, we identified several peaks, where the most abundant was corresponding to human Aβ1-42 as presented in the mass range m/z: 4300-4650 (Figure 1B). We anticipated this finding, since the human Aβ1-42 species are the main component of amyloid plaques in the tg APPPS1-21 mouse[31]. By fragmentation analysis we obtained a sufficient sequence coverage of Aβ1-42 fragment ions that, when compared to an in-silico fragmentation spectra, confirmed the presence of the Aβ1-42 peptide with multiple assigned peptide fragment ions (Supplementary Figure 2). No signal could be detected when analyzing extracts from adjacent control regions (data not shown).

In MALDI-MS, the addition of PA to the DHB matrix reduced signal suppression[5,6,12,15]. We investigated here, whether this beneficial effect was also observed when analyzing Aβ plaques. We compared PA and the standard additive, TFA, in the S-DHB matrix to investigate possible ionization difference of the Aβ plaques. The signal-to-noise (S/N) ratio of Aβ1-42 was improved two- to three-fold by PA when compared to the S-DHB matrix with TFA (PA: 31.5; TFA: 12.5; Figure 1C and 1E; Supplementary table 1). Similar improvement was found when analyzing a synthetic Aβ1-42 peptide (PA: 113.5; TFA: 59.5; Figure 1D and 1E;

Supplementary table 2). We are the first to report that the S-DHB/PA matrix provided a higher S/N ratio compared to the S-DHB/TFA matrix when analyzing both synthetic Aβ1-42 peptides and microdissected Aβ1-42 from amyloid plaques with MALDI-MS.

Brain tissue includes several ion-suppressing features that compete with ionization and interfere with MALDI imaging analysis. The S/N of the extracted plaque material (Figure 1C and 1E) was three- to four-fold lower compared to the synthetic Aβ1-42 (Figure 1D and 1E) indicating a source of signal suppression from the actual tissue. After establishing that PA addition was beneficial for MALDI-MS of Aβ1-42 peptides, we next investigated whether similar advantages with PA were present in MALDI imaging of Aβ proteoforms. PA was reported advantageous in concentration up to 1% (v/v) in MALDI-MS[6]. However, we optimized PA concentration to 0.2% in MALDI imaging, since higher acid concentrations (>1%) were deleterious for the ImagePrep setup and increased matrix wetness and analyte diffusion during matrix deposition (data not shown).

To this end, we compared brain sections from APPPS1-21 mice (Figure 2A-D) treated with S-DHB/PA or S-DHB/TFA to two matrices CHCA/TFA and SA/TFA that recently were used in MALDI imaging of Aβ proteoforms in brain tissue[28,30]. The S-DHB, CHCA and SA matrices can deteriorate over time and thus impair ionization efficiency when analyzing several tissue sections. By using a low spatial resolution, we could decrease the time necessary for analyzing the tissue sections and thus limit the influence of such bias. Linear mode is generally preferred in MALDI imaging with high spatial resolution because of the increased speed compared to the reflector mode where the TOF event is longer. We used linear mode for this analysis because of its increased analyte stability compared to reflectron mode that can affect the energetic stress during passage through the reflector. This could lead to false-positive m/z values that could match truncated Aβ species.

Several shared as well as exclusive peaks were observed in the four matrices and supported matrix dependent variance in line with previous MALDI-MS studies. The S/N level of several peaks across m/z mass range 4500 - 16000 were detected with the S-DHB matrix for PA and TFA additives (Figure 2A-B). An increased baseline in the lower region of the mass spectrum (m/z 1000 - 3000) was observed with the S-DHB/TFA matrix after sufficient top hat baseline processing favoring the PA over the TFA additive (Figure 2B). The SA matrix illustrated efficient ionization of higher molecular weight (MW) biomolecules; MW > 18 000 Da (Figure 2C). In contrast, the “hot” CHCA matrix (Figure 2D) illustrated an efficient ionization in the lower region of the mass spectra compared to the other matrices which could be explained by in-source fragmentation or post-source decay tendencies[36].

Since the Aβ1-42 peptide (including modified proteoforms) was the most abundant species observed in microdissected plaques of the APPPS1-21 mouse brain (Figure 1B), the calculated mass of Aβ1-42 ($[M+H]^{+}_{Avg}$ = 4515.1088) was selected as a marker for plaques in the MALDI imaging data analysis. We detected suboptimal ionization of Aβ1-42 with SA/TFA = 0.19 absolute intensity value (AIV) (Figure 2C) and CHCA/TFA = 0.25 AIV (Figure 2D). We detected improved signal of Aβ1-42 with S-DHB/PA = 0.54 AIV (Figure 2A; Figure 3B and 3E) and S-DHB/TFA = 0.37 AIV (Figure 2B; Figure 3B and 3E) and selected the S-DHB matrix as the most appropriate matrix with the PA additive.

The S-DHB/PA matrix provided clear visualization of Aβ1-42 and other Aβ species such as Aβ8-40, Aβ1-40 and Aβ1-43 in APPPS1-21 mouse brain tissue (Figure 3A).

When comparing the PA and TFA additives on regions of interest (ROIs) with high Aβ load from the APPPS1-21 mice, we observed a significant improvement in detection of Aβ1-42 (p = 0.0157) and Aβ1-43 (p = 0.0192) (Figure 3D). In contrast, similar AIVs were observed for Aβ8-40 and Aβ1-40 with the PA and TFA additives (Figure 3D). Our previous spectral comparison of S-DHB matrix in MALDI imaging revealed no clear difference in the lower m/z region (m/z: 1000 – 4500) whereas a clear difference was observed between the two additives for detecting peptides with higher MW (m/z > 4500) (Figure 2A and 2B). This finding from our MALDI imaging data is different from previous MALDI-MS studies where the beneficial effect of PA also was observed for peptides with lower MW (m/z > 2000) compared to TFA[15]. Taken together, the S-DHB matrix was found superior for detecting human Aβ1-42 peptides and therefore analysis of AD tissue was performed exclusively with this matrix. First, we compared detection of Aβ1-42 peptides in one postmortem AD brain comparing PA and TFA additives. The advantageous effect of PA was more pronounced in tissue from AD compared to APPPS1-21 brain tissue. We observed a two- to three-fold improvement of AIV with PA = 0.88 vs TFA = 0.31 for Aβ1-42 detection in AD brain tissue (Figure 3C and 3E). Interestingly, the improved effect was also observed for detection of pyroglutamate-modified Aβ1-42 (N3pE42; Figure 3E).

The sensitivity gain by PA in MALDI-MS was hypothesized to be caused by an increased ionic strength upon evaporation of solvent that is incorporated into the matrix[5,6]. In MALDI imaging, the observed improvement of the S/N ratio, specifically in the AD brain tissue, could be additionally explained by the capability of S-DHB/PA to limit effects of interfering molecules such as lipids and salts known to cause signal suppression.

Aβ1-42 co-localizing peptides in AD and tg mouse tissue

Various Aβ species including different truncations and posttranslational modifications associate with AD plaques[17–19]. Taking advantage of the optimized detection-method of the S-DHB matrix with PA as matrix additive, we analyzed the presence of low abundant analytes that co-localized with Aβ1-42. We merged 27 spots from the APPPS1-21 mice to create an enriched mouse Aβ1-42 mass spectrum (Figure 4A).

This approach revealed several m/z values corresponding to the calculated mass of other murine (m) and human Aβ species, including mAβ11-42, Aβ8-40, Aβ1-38, mAβ1-40, Aβ1-40, mAβ1-42, Aβ1-42, Aβ1-42 oxidized (Ox), Aβ1-43, Aβ1-43 Ox (Figure 4A). Most human Aβ species detected in the APPPS1-21 mice were full-length except for Aβ8-40 which was N-terminal truncated. In contrast, when analyzing five postmortem AD brains to create an enriched human Aβ mass spectrum (n = 30 spots; Figure 4B), we detected mostly N-truncated Aβ species. Oxidized and N-truncated species, including pyroglutamate-modified peptides (NXpEX), were detected in AD brains previously[30,37–40]. All five AD samples showed spectral similarities of Aβ species matching Aβ1-29, N11pE42, Aβ11-42, N11pE43, Aβ1-31, Aβ10-42, Aβ9-42, Aβ1-32, Aβ8-42, Aβ8-42Ox, Aβ1-33, Aβ8-43, Aβ7-42, Aβ7-43, Aβ6-42, Aβ5-42, N3pE40, Aβ4-42, N3pE42, Aβ1-40, Aβ2-42, Aβ1-42, Aβ1-42 Ox, Aβ1-43, Aβ1-43 Ox.
Variants such as Aβ1-40 and Aβ1-43 were detected in the enriched Aβ1-42 mass spectra from both tg mouse and AD (Figure 4) but we found a more complex co-localization in AD compared to the APPPS1-21 mouse brains. The major difference was the degree of N-truncated Aβ species in AD (Figure 4B). However, we cannot exclude that the level of N-terminal truncation could increase with progressing age in the APPPS1-21 mice. In another tg mouse strain (APP23) pyroglutamate-modified Aβ peptides were detectable in older mice at 24-month of age[41].
We observed a particular ratio in all five AD samples between N3pE42, Aβ1-40 and Aβ1-42 which was not detected in the 9-month old APPPS1-21 mice. Since the S-DHB/PA matrix favored the Aβ1-42 and N3pE42 compared to Aβ1-40 peptides (Figure 3C), we asked whether this ratio was derived from the use of the S-DHB/PA matrix. However, this ratio of high Aβ1-42 and N3pE42 and low Aβ1-40 was also observed previously in AD brains analyzed with a different matrix than S-DHB/PA and use of formic acid (FA) pretreatment[30]. We detected pyroglutamate-modified Aβ species using PA as matrix additive and without FA pretreatment, suggesting that the observed ratio between high Aβ1-42 and N3pE42 and low Aβ1-40 is

unlikely to be dependent on the S-DHB/PA matrix and could reflect the actual amyloid plaque composition in AD.

Aβ1-42 species form the senile plaque core while Aβ1-40 species are accumulating in the vasculature as main component in amyloidosis[42,43]. We identified the pyroglutamate-modified Aβ peptides as a noticeable component co-localized with Aβ1-42 in AD brains. Apart from the prominent N3pE42, we also observed similar intensity of a co-localizing peak matching N11pE-42. We speculate that the hydrophobicity of Aβ1-42 (defined by the C-terminus) determines that the N-terminal part is accessible to truncation and modification by glutaminyl cyclase to generate the pyroglutamate-modification. This modification renders Aβ peptides resistant to protein degradation and could explain the higher abundancy of the N3pE-42 and N11pE-42 co-localized with Aβ1-42 (the main constituent of amyloid plaques in AD brains). N-truncation and modified Aβ species are believed to be disease relevant and thus detailed identification and detection by MALDI imaging of such complex composition will help understanding the underlying disease pathology in AD.

Conclusions

Enrichment of Aβ plaques by laser microdissection was critical for detailed analysis. Head-to-head comparison of commonly used matrices revealed improved detection of Aβ1-42 with PA as matrix additive to the S-DHB matrix in MALDI imaging. Reduction of signal suppression by PA was especially advantageous when identifying complex plaque composition from AD brains. We recommend a parallel strategy of using laser microdissection and MALDI imaging with an enhanced matrix to limit ion suppression effects and increase the detection rate of Aβ plaque-associated peptides.

References

1. Gessel MM, Norris JL, Caprioli RM, Sanchez J. MALDI imaging mass spectrometry: Spatial molecular analysis to enable a new age of discovery. *J Proteomics*. 2014;107:71-82. doi:10.1016/j.jprot.2014.03.021

2. Anderson DMG, Van de Plas R, Rose KL, et al. 3-D imaging mass spectrometry of protein distributions in mouse Neurofibromatosis 1 (NF1)-associated optic glioma. *J Proteomics*. 2016;149:77-84. doi:10.1016/j.jprot.2016.02.004

3. Kratzer R, Eckerskorn C, Karas M, Lottspeich F. Suppression effects in enzymatic peptide ladder sequencing using ultraviolet-matrix assisted laser desorption/ionization-mass spectrometry. *Electrophoresis*. 1998;19(11):1910–1919. doi:10.1002/elps.1150191109

4. Norris JL, Caprioli RM. Analysis of tissue specimens by matrix-assisted laser desorption/ionization imaging mass spectrometry in biological and clinical research. *Chem Rev*. 2013;113(4):2309-2342. doi:10.1021/cr3004295

5. Stensballe A, Jensen ON. Phosphoric acid enhances the performance of Fe (III) affinity chromatography and matrix-assisted laser desorption / ionization tandem mass spectrometry for recovery , detection and sequencing of phosphopeptides. *Rapid Commun Mass Spectrom*. 2004;18(15):1721-1730. doi:10.1002/rcm.1542

6. Kjellstrtöm S, Jensen ON. Phosphoric acid as a matrix additive for MALDI MS analysis of phosphopeptides and phosphoproteins. *Anal Chem*. 2004;76(17):5109-5117. doi:10.1021/ac0400257

7. Beavis RC, Chait BT, Standing KG. Matrix-assisted laser-desorption mass spectrometry using 355 nm radiation. *Rapid Commun Mass Spectrom*. 1989;3(12):436-439. doi:10.1002/rcm.1290031208

8. Beavis RC, Chaudhary T, Chait BT. α-Cyano-4-hydroxycinnamic acid as a matrix for matrixassisted laser desorption mass spectromtry. *Org Mass Spectrom*. 1992;27:156-158. doi:10.1002/oms.1210270217

9. Strupat K, Karas M, Hillenkamp F. 2,5-Dihydroxybenzoic acid: a new matrix for laser desorption-ionization mass spectrometry. *Int J Mass Spectrom Ion Process*. 1991;111:89-102. doi:10.1016/0168-1176(91)85050-V

10. Cohen SL, Chait BT. Influence of matrix solution conditions on the MALDI-MS analysis of peptides and proteins. *Anal Chem*. 1996;68(1):31-37. doi:10.1021/ac9507956

11. Laugesen S, Roepstorff P. Combination of Two Matrices Results in Improved Performance of MALDI MS for Peptide Mass Mapping and Protein Analysis. *Am Soc Mass Spectrom*. 2003;14(9):992-1002. doi:10.1016/S1044-0305(03)00262-9

12. Kuyama H, Sonomura K, Nishimura O. Sensitive detection of phosphopeptides by matrix-assisted laser desorption / ionization mass spectrometry : use of alkylphosphonic acids as matrix additives. *Rapid Commun Mass Spectrom*. 2008;22(8):1109-1116. doi:10.1002/rcm.3482

13. Rosinke B, Stropat K, Hillenkamp F, et al. Matrix-Assisted Laser Desorption/Ionization Mass Spectrometry (MALDI-MS) of Membrane Proteins and Non-covalent Complexes. *J Mass Spectrom*. 1995;30(10):1462-1468. doi:10.1002/jms.1190301012

14. Pfenninger A, Karas M, Finke B, Stahl B, Sawatzki G. Matrix Optimization for Matrix-assisted Laser Desorption/Ionization Mass Spectrometry of Oligosaccharides from Human Milk. *J Mass Spectrom*. 1999;34(2):98-104. doi:10.1002/(SICI)1096-9888(199902)34:2<98::AID-JMS767>3.0.CO;2-N

15. Park S, Kim T, Lee J, Seo M, Kim J. Effect of phosphoric acid as a matrix additive in matrix-assisted laser desorption/ionization analysis. *Rapid Commun Mass Spectrom*. 2013;27(7):842-846. doi:10.1002/rcm.6508

16. Hardy J, Selkoe DJ. The Amyloid Hypothesis of Alzheimer ' s Disease : Progress and Problems on the Road to Therapeutics. *Science*. 2002;297(5580):353-356. doi:10.1126/science.1072994

17. Masters CL, Simms G, Weinman NA, Multhaupt G, Mcdonald BL. Amyloid plaque core protein in Alzheimer disease and Down syndrome. *Proc Natl Acad Sci USA*. 1985;82(12):4245-4249. doi:10.1073/pnas.82.12.4245

18. Selkoe DJ. The Molecular of Alzheimer's Pathology Disease Review. *Neuron*. 1991;6(4):487-498. doi:10.1016/0896-6273(91)90052-2

19. Hardy JA, Higgins GA. Alzheimer's Disease: The Amyloid Cascade Hypothesis.

Science. 1992;256(5054):184-185.

20. Haass C, Selkoe DJ. Soluble protein oligomers in neurodegeneration: lessons from the Alzheimer's amyloid β-peptide. *Nat Rev Mol Cell Biol*. 2007;8(2):101-112. doi:10.1038/nrm2101

21. Walsh DM, Selkoe DJ. Deciphering the Molecular Basis of Memory Failure in Alzheimer's Disease. *Neuron*. 2004;44(1):181-193. doi:10.1016/j.neuron.2004.09.010

22. Esquerda-canals G, Montoliu-Gaya L, Güell-Bosch J, Villegas S. Mouse Models of Alzheimer's Disease. *J Alzheimer's Dis*. 2017;57(4):1171-1183. doi:10.3233/JAD-170045

23. Stoeckli M, Staab D, Staufenbiel M, Wiederhold K, Signor L. Molecular imaging of amyloid β peptides in mouse brain sections using mass spectrometry. *Anal Biochem*. 2002;311(1):33-39. doi:10.1016/S0003-2697(02)00386-X

24. Stoeckli M, Knochenmuss R, McCombie G, et al. MALDI MS imaging of amyloid. *Methods Enzymol*. 2006;412:94-106. doi:10.1016/S0076-6879(06)12007-8

25. Rohner TC, Staab D, Stoeckli M. MALDI mass spectrometric imaging of biological tissue sections. *Mech Ageing Dev*. 2005;126(1):177-185. doi:10.1016/j.mad.2004.09.032

26. Kelley AR, Perry G, Bethea C, Castellani RJ, Bach SBH. Molecular Mapping Alzheimer's Disease: MALDI Imaging of Formalin-fixed, Paraffin-embedded Human Hippocampal Tissue. *Open Neurol J*. 2016;10:88-98. doi:10.2174/1874205X01610010088

27. Kelley AR, Perry G, Castellani RJ, Bach SBH. Laser-Induced In-Source Decay Applied to the Determination of Amyloid-Beta in Alzheimer's Brains. *ACS Chem Neurosci*. 2016;7(3). doi:10.1021/acschemneuro.5b00295

28. Carlred L, Michno W, Kaya I, Sjövall P, Syvänen S, Hanrieder J. Probing amyloid-β pathology in transgenic Alzheimer's disease (tgArcSwe) mice using MALDI imaging mass spectrometry. *J Neurochem*. 2016;138(3):469-478. doi:10.1111/jnc.13645

29. Kaya I, Brinet D, Michno W, Zetterberg H, Blenow K. Novel Trimodal MALDI Imaging Mass Spectrometry (IMS3) at 10 μm Reveals Spatial Lipid and Peptide Correlates

Implicated in Aβ Plaque Pathology in Alzheimer ’s Disease. *ACS Chem Neurosci*. 2017;8(12):2778-2790. doi:10.1021/acschemneuro.7b00314

30. Kakuda N, Miyasaka T, Iwasaki N, Nirasawa T, Wada-kakuda S. Distinct deposition of amyloid-β species in brains with Alzheimer’s disease pathology visualized with MALDI imaging mass spectrometry. *Acta Neuropathol Commun*. 2017;5(73):1-8. doi:10.1186/s40478-017-0477-x

31. Radde R, Bolmont T, Kaeser SA, et al. Aβ42-driven cerebral amyloidosis in transgenic mice reveals early and robust pathology. *EMBO Rep*. 2006;7(9):940-946. doi:10.1038/sj.embor.7400784

32. Braak H, Braak E. Neuropathological stageing of Alzheimer-related changes. *Acta Neuropathol*. 1991;82(4):239-259. doi:10.1007/BF00308809

33. Yang J, Caprioli RM. Matrix Sublimation/Recrystallization for Imaging Proteins by Mass Spectrometry at High Spatial Resolution. *Anal Chem*. 2011;83(14):5728-5734. doi:10.1021/ac200998a

34. Axelsen T, Holm A, Birkelund S, Christiansen G, Ploug M, Holm I. Specific recognition of the C-terminal end of Aβ42 by a high affinity monoclonal antibody. *Mol Immunol*. 2009;46(11-12):2267-2273. doi:10.1016/j.molimm.2009.04.007

35. Vizcaíno JA, Csordas A, Del-Toro N, et al. 2016 update of the PRIDE database and its related tools. *Nucleic Acids Res*. 2016;44(D1):D447-D456. doi:10.1093/nar/gkv1145

36. Karas M, Bahr U, Strupat K, Hillenkamp F, Tsarbopoulos A, Pramanik BN. Matrix Dependence of Metastable Fragmentation of Glycoproteins in MALDI TOF Mass Spectrometry. *Anal Chem*. 1995;67(3):675-679. doi:10.1021/ac00099a029

37. Liu K, Solano I, Mann D, et al. Characterization of Aβ11-40/42 peptide deposition in Alzheimer’s disease and young Down’s syndrome brains: implication of N-terminally truncated Aβ species in the pathogenesis of Alzheimer’s disease. *Acta Neuropathol*. 2006;112(2):163-174. doi:10.1007/s00401-006-0077-5

38. Güntert A, Döbeli H, Bohrmann B. High sensitivity analysis of amyloid-beta peptide composition in amyloid deposits from human and PS2APP mouse brain. *Neuroscience*. 2006;143(2):461-475. doi:10.1016/j.neuroscience.2006.08.027

39. Rüfenacht P, Güntert A, Bohrmann B, Ducret A, Döbeli H. Quantification of the Aβ pepticle in Alzheimer's plaques by laser dissection microscopy combined with mass spectrometry. *J Mass Spectrom*. 2005;40(2):193-201. doi:10.1002/jms.739

40. Moore BD, Chakrabarty P, Levites Y, et al. Overlapping profiles of Aβ peptides in the Alzheimer's disease and pathological aging brains. *Alzheimer's Res Ther*. 2012;4(3):121. doi:10.1186/alzrt121

41. Schieb H, Kratzin H, Jahn O, et al. β-Amyloid Peptide Variants in Brains and Cerebrospinal Fluid from Amyloid Precursor Protein (APP) Transgenic Mice. *J Biol Chem*. 2011;286(39):33747-33758. doi:10.1074/jbc.M111.246561

42. Iwatsubo T, Odaka A, Suzuki N, Mizusawa H, Nukina N, Ihara Y. Visualization of Aβ42(43) and Aβ40 in senile plaques with end-specific Aβ monoclonals: Evidence that an initially deposited species is Aβ42(43). *Neuron*. 1994;13(1):45-53. doi:10.1016/0896-6273(94)90458-8

43. Gravina SA, Ho L, Eckman CB, et al. Amyloid β protein (Aβ) in Alzheimer's disease brain. Biochemical and immunocytochemical analysis with antibodies specific for forms ending at Aβ40 or Aβ42(43). *J Biol Chem*. 1995;270(13):7013-7016. doi:10.1074/jbc.270.13.7013

Table 1: Average values acquired from the matrix deposition of mouse brain tissue.

	DHB/ 0.2% PA	**DHB/ 0.2% TFA**	**SA/ 0.2% TFA**	**CHCA/ 0.2% TFA**
Average deposition layer (Light scattering intensity)	4.7	4.3	3.3	4.1
Average deposition time (Minutes)	94	75	58	60

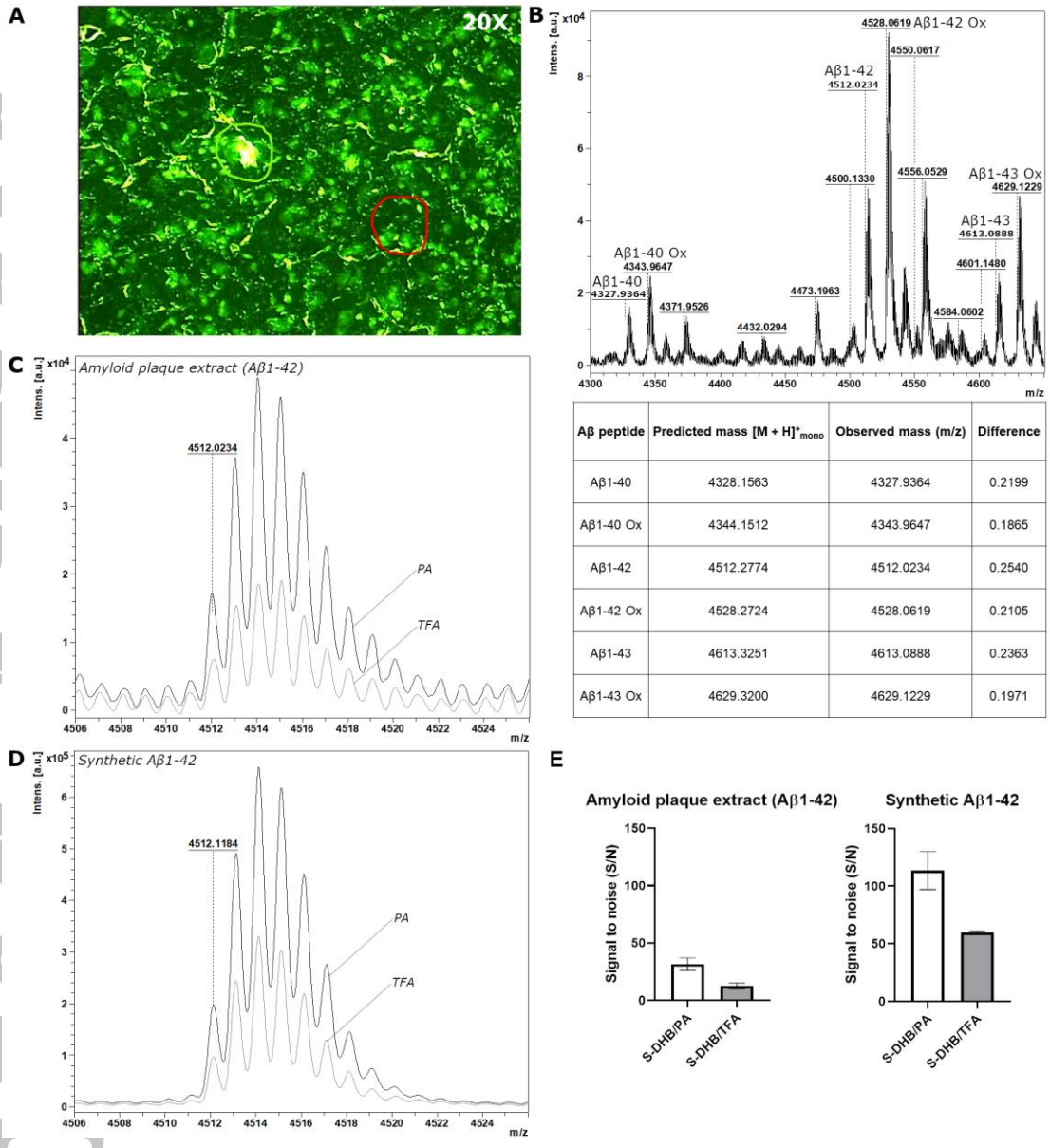

Aβ peptide	Predicted mass $[M + H]^+_{mono}$	Observed mass (m/z)	Difference
Aβ1-40	4328.1563	4327.9364	0.2199
Aβ1-40 Ox	4344.1512	4343.9647	0.1865
Aβ1-42	4512.2774	4512.0234	0.2540
Aβ1-42 Ox	4528.2724	4528.0619	0.2105
Aβ1-43	4613.3251	4613.0888	0.2363
Aβ1-43 Ox	4629.3200	4629.1229	0.1971

Figure 1: Improved detection of beta-amyloid (Aβ) species by phosphoric acid (PA) matrix additive in MALDI-MS. A) Thioflavin-T staining of APPPS1-21 brain tissue section prior to laser capture microdissection. A plaque is highlighted with a green circle and an adjacent control area is highlighted with a red circle. The image was acquired with a 20X objective lens. B) Mass spectrum acquired from microdissected APPPS1-21 plaque material. Data was acquired in positive ion reflectron mode; mass range: m/z 4300-4650. Identified peaks were calculated to Aβ1-40, Aβ1-40 Oxidation (Ox; M+16), Aβ1-42, Aβ1-42 Ox, Aβ1-43 and Aβ1-43 Ox. The observed and calculated m/z, including differences, are presented in the associated table. C) Signal-to-noise (S/N) comparison of extracted plaque material from APPPS1 mice using the DHB/PA matrix (black) or S-DHB/TFA matrix (grey). D) S/N comparison of synthetic amyloid beta (Aβ)1-42 peptide using the SDHB/PA matrix (black) or S-DHB/TFA matrix (grey). Mass range in C) and D) = m/z 4506 - 4526. E) Representation of mean S/N (mean ± s.e.m; n = two replicates).

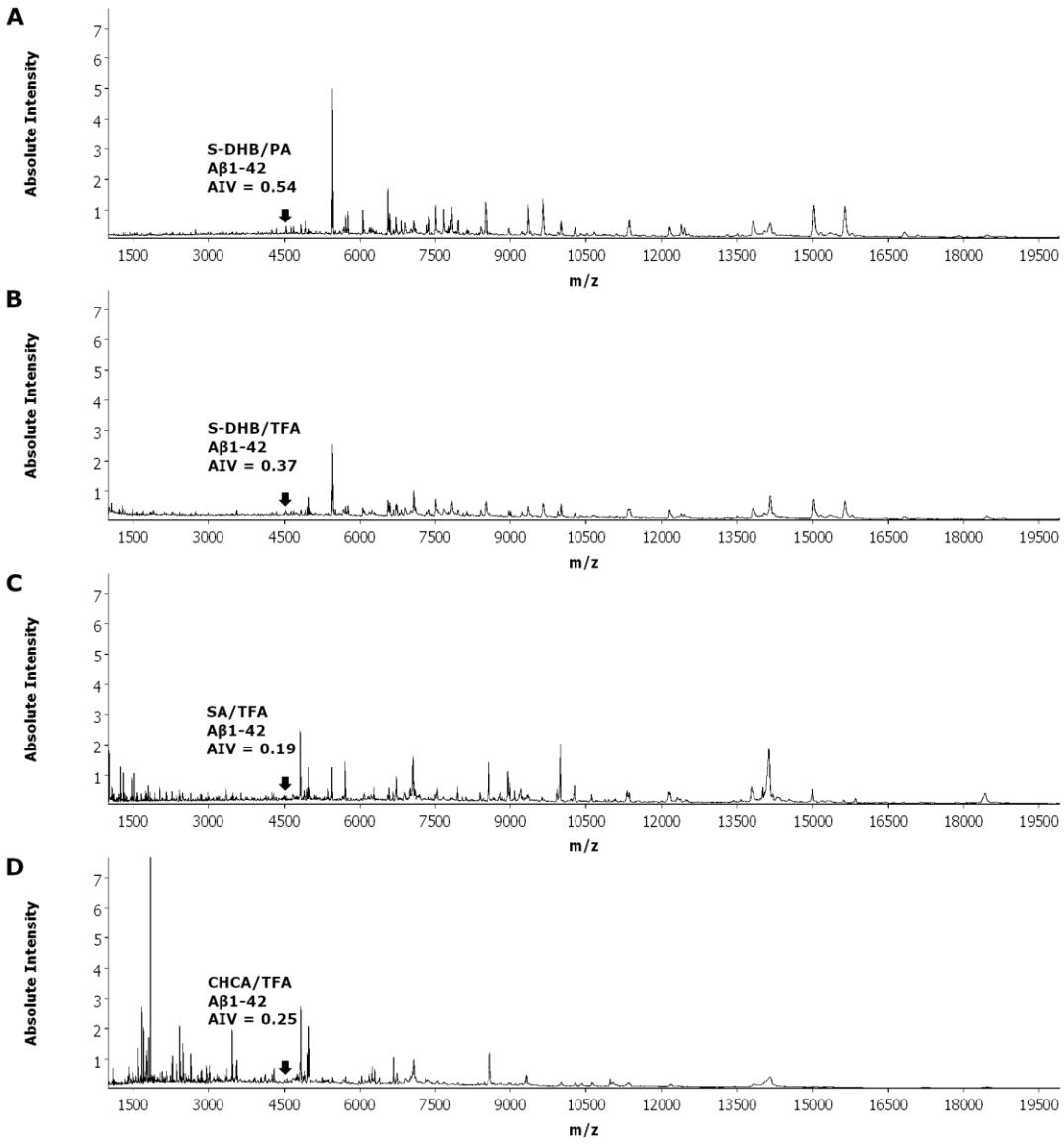

Figure 2: Matrix comparison in MALDI imaging. Processed and normalized mass spectra at different matrix conditions. Each mass spectrum is an average of nine tissue sections (three tissue sections per APPPS1-21 mouse brain). A) S-DHB/PA matrix. B) S-DHB/TFA matrix. C) SA/TFA matrix. D) CHCA/TFA matrix. Mass spectra are visualized with absolute intensities at mass range: m/z 1000-20000. AIV = absolute intensity value. The position of the beta-amyloid (Aβ)1-42 peptide is visualized with an arrow.

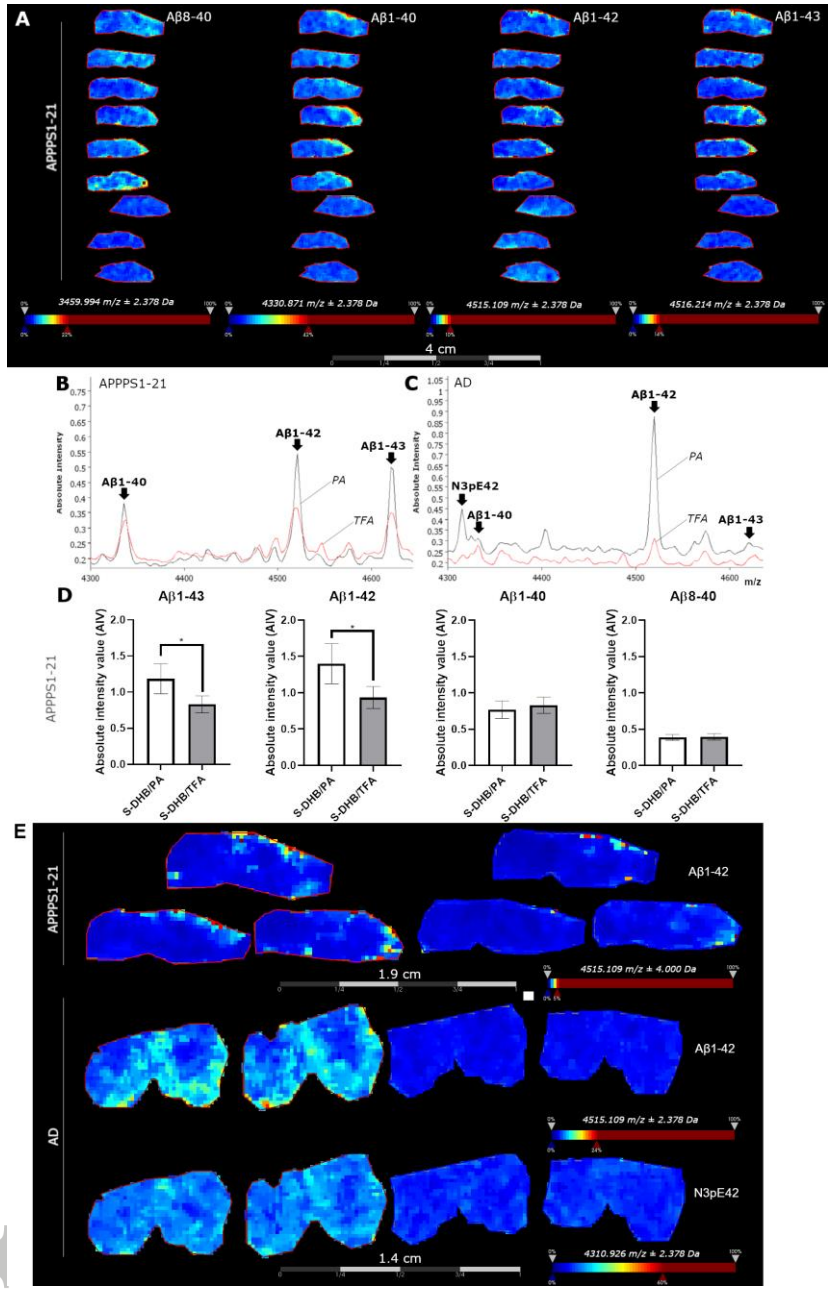

Figure 3: Improved detection of beta-amyloid (Aβ) species from APPPS1-21 and AD brain tissue by phosphoric acid (PA) matrix additive in MALDI imaging. A) Single ion images of beta-amyloid (Aβ) peptide species (Aβ8-40, Aβ1-40, Aβ1-42, Aβ1-43) with MALDI imaging (linear mode; 300 µm resolution; S-DHB/PA matrix; weak denoising; n = three APPPS1-21 mice (three sections per mouse brain); Scale bar = 4 cm). B) Absolute intensity spectra of Aβ1-42 when using S-DHB/PA (black) and S-DHB/TFA (red) on APPPS1-21 mouse brain tissue (n = 9). C) Absolute intensity spectra of Aβ1-42 when using S-DHB/PA (black) and S-DHB/TFA (red) on Alzheimer's disease (AD) brain tissue (n = 2). D) Absolute intensity values (AIVs) of Aβ1-43, Aβ1-42, Aβ1-40 and Aβ8-40 proteoforms in selected ROIs when using PA and TFA matrix additives on APPPS1-21 mouse brain tissue. Data represent mean ± s.e.m.; Paired t-test, *p < 0,05; n = 9. E) Single ion images of Aβ1-42 (4515.109 m/z) and pyroglutamate-modified Aβ1-42 (Np3E42; 4310.926 m/z) in APPPS1-21 (upper) and AD (lower) brain tissue when using S-DHB with PA (left) or TFA (right) matrix additive (300 and 200 µm resolution for mouse and AD tissue, respectively; weak denoising; Scale bar = 1.9 and 1.4 cm, respectively.

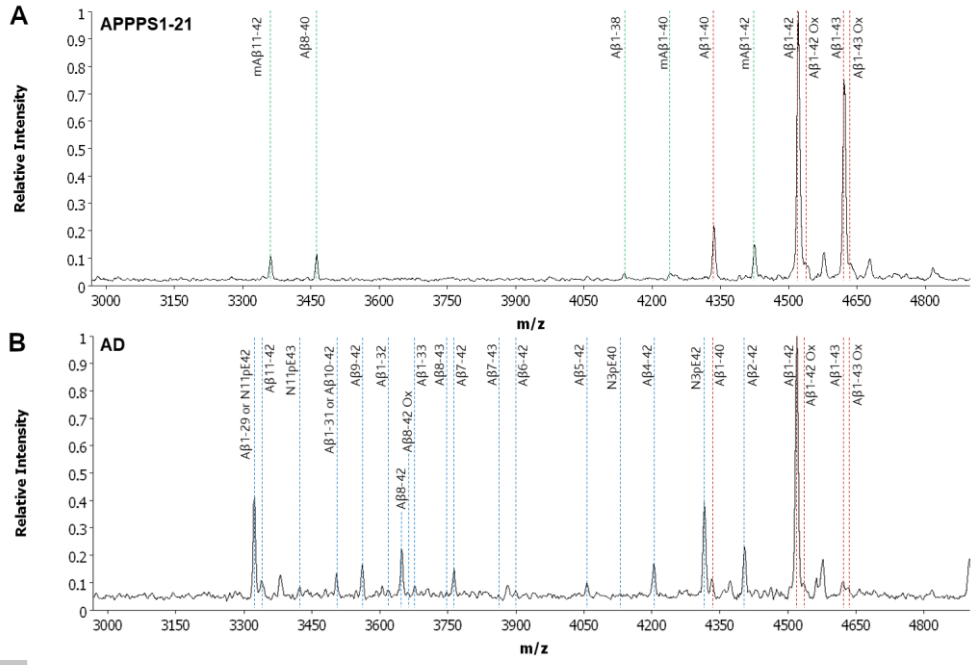

Figure 4: Enriched Aβ1-42 mass spectrum from transgenic APPPS1-21 mouse and Alzheimer's disease (AD) brain tissue. A) Enriched Aβ1-42 mass spectrum from transgenic APPPS1-21 mouse brain tissue (n = 27 spots; from 3 APPPS1-21 mice). Identified peaks were calculated to murine (m)Aβ11-42, Aβ8-40, Aβ1-38, mAβ1-40, Aβ1-40, mAβ1-42, Aβ1-42, Aβ1-42 oxidized (Ox; M + 16), Aβ1-43, Aβ1-43 Ox. B) Enriched Aβ1-42 mass spectrum from Alzheimer's disease (AD) brain tissue (n = 30 spots; five AD patients). Identified peaks were calculated to Aβ1-29, pyroglutamate modified Aβ (NXpEX) N11pE42, Aβ11-42, N11pE43, Aβ1-31, Aβ10-42, Aβ9-42, Aβ1-32, Aβ8-42, Aβ8-42 Ox, Aβ1-33, Aβ8-43, Aβ7-42, Aβ7-43, Aβ6-42, Aβ5-42, N3pE40, Aβ4-42, N3pE42, Aβ1-40, Aβ2-42, Aβ1-42, Aβ1-42 Ox, Aβ1-43, Aβ1-43 Ox. The data was acquired in linear mode; m/z 1000-20000; S-DHB/PA matrix. Aβ proteoforms exclusive to mouse and human are indicated by dotted green and blue lines, respectively. Shared peaks are indicated by dotted red lines.